Optics Letters

Plasmon coherence determination by nanoscattering

Yahong Chen,[1,2,*] Andreas Norrman,[1,3] Sergey A. Ponomarenko,[4] and Ari T. Friberg[1]

[1]Institute of Photonics, University of Eastern Finland, P.O. Box 111, FI-80101 Joensuu, Finland
[2]College of Physics, Optoelectronics and Energy & Collaborative Innovation Center of Suzhou Nano Science and Technology, Soochow University, Suzhou 215006, China
[3]Max Planck Institute for the Science of Light, Staudtstraße 2, D-91058 Erlangen, Germany
[4]Department of Electrical and Computer Engineering, Dalhousie University, Halifax, Nova Scotia, B3J 2X4, Canada
*Corresponding author: hon2019@163.com

Received 30 June 2017; revised 20 July 2017; accepted 20 July 2017; posted 20 July 2017 (Doc. ID 301066); published 17 August 2017

We present a simple and robust protocol to recover the second-order field correlations of polychromatic, statistically stationary surface plasmon polaritons (SPPs) from a spectrum measurement in the far zone of a dipolar nanoscatterer. The recovered correlations carry comprehensive information about the spectral, spatial, and temporal coherence of the SPPs. We also introduce and exemplify for the first time, to the best of our knowledge, the two-point Stokes parameters associated with partially coherent SPP fields.

OCIS codes: (030.1640) Coherence; (240.6680) Surface plasmons; (260.2110) Electromagnetic optics.

https://doi.org/10.1364/OL.42.003279

Due to its unique properties, the celebrated surface plasmon polariton (SPP) [1] has been in the spotlight in nanophotonics [2] and led to the advent of modern plasmonics [3], involving a broad range of interdisciplinary science and engineering [4–11]. Despite its success, however, to date plasmonics has mainly concerned fully coherent SPP phenomena. Surface plasmons are nonetheless known to play key roles in modifying the coherence properties of light traversing nanoscale structures in metal films [12–15], they form key elements of plasmonic interferometers to measure subwavelength coherences [16], and they affect significantly the coherence [17], spectrum [18], and polarization [19] of thermal near fields. Thus, exploring electromagnetic coherence under SPP excitation is of great interest, not the least from an applications point of view, as coherence provides a fundamental degree of freedom to control spectral distribution, propagation, interference, polarization, and various electromagnetic interactions [20]. Yet, whereas the above studies deal with SPP-induced coherence, very little research has been devoted to investigate the SPP coherence itself [21–23].

Recently, a general theoretical framework to tailor the electromagnetic coherence of polychromatic SPPs excited in the Kretschmann configuration was formulated [24]. Within this framework, all SPP coherence properties are specified by a single spectral correlation function which, in turn, can be controlled by judiciously engineering the coherence state of the excitation light. Such a procedure, which we call plasmon coherence engineering, however, requires precise control of the source correlations. Hence, it is natural to enquire whether there is another way to determine the SPP coherence characteristics. In this Letter, we demonstrate that the electromagnetic coherence of a statistically stationary SPP field can be assessed from just a single spectrum measurement. We specifically show that all second-order correlation properties of the SPP field, in principle, can be completely recovered by measuring the far-field spectrum scattered by a nanoparticle placed in the vicinity of the metal surface. We also introduce the two-point Stokes parameters [25,26] of such partially coherent SPPs and illustrate by physical examples the information they provide about the intrinsic structure of the SPP-field coherence.

We consider a polychromatic SPP field in the Kretschmann setup (see Fig. 1), excited by a TM-polarized, statistically stationary light beam with tailored coherence properties [24]. The homogenous, isotropic, and nonmagnetic metal film, deposited

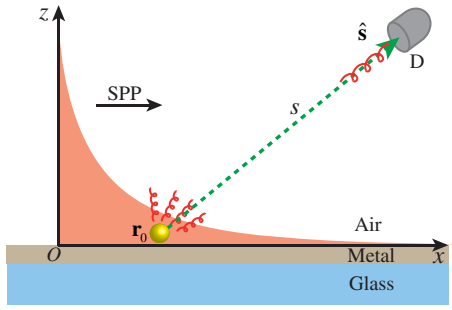

Fig. 1. Schematic of the nanoscattering setup associated with the determination of the statistical properties of a polychromatic, partially coherent SPP field in the Kretschmann configuration. The geometry and the SPP field are uniform in the y direction. The nanoparticle is located at point $\mathbf{r}_0$ near the metal surface $z = 0$, and the scattered far field is observed by detector D at a distance s in the direction $\hat{\mathbf{s}}$ from $\mathbf{r}_0$.

on a glass prism and located in the xy plane, is characterized by a complex-valued relative permittivity $\epsilon_r(\omega)$, accounting for dispersion and absorption. The film is thick enough to prevent coupling between the modes at the two metal surfaces. We take the x axis to represent the SPP propagation direction and $z = 0$ to coincide with the planar metal–air boundary. Under these circumstances, the spatial electric part of an SPP in air, at point $\mathbf{r}$ and (angular) frequency ω, can be expressed as [27]

$$\mathbf{E}(\mathbf{r}, \omega) = E(\omega)\hat{\mathbf{p}}(\omega)e^{i\mathbf{k}(\omega)\cdot\mathbf{r}}, \tag{1}$$

where $E(\omega)$ is the complex-valued field amplitude at the origin ($\mathbf{r} = 0$), and [28]

$$\mathbf{k}(\omega) = k_x(\omega)\hat{\mathbf{e}}_x + k_z(\omega)\hat{\mathbf{e}}_z, \quad \hat{\mathbf{p}}(\omega) = [\mathbf{k}(\omega) \times \hat{\mathbf{e}}_y]/|\mathbf{k}(\omega)| \tag{2}$$

are the wave vector and unit polarization vector, respectively, with $\hat{\mathbf{e}}_x$, $\hat{\mathbf{e}}_y$, and $\hat{\mathbf{e}}_z$ being the Cartesian unit vectors. The wave vector components in Eq. (2), which follow directly from the electromagnetic boundary conditions, read as [1,2]

$$k_x(\omega) = \frac{\omega}{c}\sqrt{\frac{\epsilon_r(\omega)}{\epsilon_r(\omega)+1}}, \quad k_z(\omega) = \frac{\omega}{c}\sqrt{\frac{1}{\epsilon_r(\omega)+1}}, \tag{3}$$

in which c is the speed of light in vacuum.

On taking $\mathbf{E}(\mathbf{r}, \omega)$ in Eq. (1) as a field realization, we can express the spectral electric coherence matrix characterizing the random SPP field as $\mathbf{W}(\mathbf{r}_1, \mathbf{r}_2, \omega) = \langle \mathbf{E}^*(\mathbf{r}_1, \omega)\mathbf{E}^{\mathrm{T}}(\mathbf{r}_2, \omega)\rangle$ [29], where the asterisk and superscript T denote complex conjugate and matrix transpose, respectively, and the angle brackets stand for the ensemble average. Explicitly, according to Eqs. (1) and (2),

$$\mathbf{W}(\mathbf{r}_1, \mathbf{r}_2, \omega) = W(\omega)\mathbf{K}(\omega)e^{i[\mathbf{k}(\omega)\cdot\mathbf{r}_2 - \mathbf{k}^*(\omega)\cdot\mathbf{r}_1]}, \tag{4}$$

which includes the spectral distribution function

$$W(\omega) = \langle |E(\omega)|^2 \rangle, \tag{5}$$

and the Hermitian matrix (specified by spectral polarization)

$$\mathbf{K}(\omega) = \hat{\mathbf{p}}^*(\omega)\hat{\mathbf{p}}^{\mathrm{T}}(\omega) = \frac{1}{|\mathbf{k}(\omega)|^2}\begin{bmatrix} |k_z(\omega)|^2 & -k_z^*(\omega)k_x(\omega) \\ -k_x^*(\omega)k_z(\omega) & |k_x(\omega)|^2 \end{bmatrix}. \tag{6}$$

The temporal electric coherence matrix of the stationary SPPs is obtained via the (generalized) Wiener–Khintchine theorem [20]

$$\mathbf{\Gamma}(\mathbf{r}_1, \mathbf{r}_2, \tau) = \int_0^\infty \mathbf{W}(\mathbf{r}_1, \mathbf{r}_2, \omega)e^{-i\omega\tau}d\omega, \tag{7}$$

where $\tau = t_2 - t_1$ is a time delay. An important point to note here is that, for a given metal, the spectral and temporal SPP coherence matrices are entirely specified by the single spectral function $W(\omega)$.

We demonstrate next how the function $W(\omega)$ and, thereby, all the second-order statistical properties of the SPP field can be determined by measuring the spectrum of the far field scattered by a nanoparticle. To this end, we consider a spherical metallic nanoprobe in close vicinity of the metal slab at a point $\mathbf{r}_0 = x_0\hat{\mathbf{e}}_x + z_0\hat{\mathbf{e}}_z$ (see Fig. 1), with the radius taken to be much smaller than the minimum wavelength and the minimum penetration depth within the SPP bandwidth. Thus, the scattering can be treated in the electrostatic dipole approximation [1]. The radiated far field in the xz plane, at a distance s in the direction $\hat{\mathbf{s}} = \mathbf{s}/s$ (measured from $\mathbf{r}_0$), is given by

$$\mathbf{E}_\infty(\mathbf{r}, \omega) = \left(\frac{\omega^2}{4\pi c^2\epsilon_0}\right)\hat{\mathbf{s}} \times [\mathbf{d}(\mathbf{r}_0, \omega) \times \hat{\mathbf{s}}]\frac{e^{i(\omega/c)s}}{s}, \tag{8}$$

where ϵ_0 is the vacuum permittivity, and $\mathbf{d}(\mathbf{r}_0, \omega)$ is the dipole moment of the scatterer. In the electrostatic regime, $\mathbf{d}(\mathbf{r}_0, \omega)$ is directly proportional to the SPP field via [1]

$$\mathbf{d}(\mathbf{r}_0, \omega) = \alpha(\omega)\mathbf{E}(\mathbf{r}_0, \omega), \quad \alpha(\omega) = 4\pi\epsilon_0\frac{\epsilon_r(\omega) - 1}{\epsilon_r(\omega) + 2}a^3, \tag{9}$$

in which $\alpha(\omega)$ is the polarizability, $\epsilon_r(\omega)$ is the relative permittivity, and a is the radius of the nanosphere. We point out that Eqs. (8) and (9) neglect effects due to the presence of the metal surface. In particular, $\alpha(\omega)$ will be replaced by an effective polarizability $\alpha_{\mathrm{eff}}(\omega)$, and $\mathbf{E}_\infty(\mathbf{r}, \omega)$ acquires an additional contribution from the metal reflection. These effects can readily be included in a quantitative analysis and in experiments (see, e.g., [30] and the references therein), and they will not impact the main conclusions below.

In polar coordinates, with θ being the angle between $\hat{\mathbf{s}}$ and the x axis, Eqs. (8) and (9) result in the far-field expression

$$\mathbf{E}_\infty(\mathbf{r}, \theta, \omega) = \left(\frac{\omega^2}{4\pi c^2\epsilon_0}\right)\alpha(\omega)\mathbf{M}(\theta)\mathbf{E}(\mathbf{r}_0, \omega)\frac{e^{i(\omega/c)s}}{s}, \tag{10}$$

where we have introduced the symmetric matrix

$$\mathbf{M}(\theta) = \begin{bmatrix} \sin^2\theta & -\sin\theta\cos\theta \\ -\sin\theta\cos\theta & \cos^2\theta \end{bmatrix}. \tag{11}$$

Employing Eq. (10), together with the property $\mathbf{M}^2(\theta) = \mathbf{M}(\theta)$, one finds that the spectrum of the scattered field in the far zone at point $\mathbf{r}$ takes on the form

$$S_\infty(\mathbf{r}, \theta, \omega) = \mathrm{tr}[\langle \mathbf{E}_\infty^*(\mathbf{r}, \theta, \omega)\mathbf{E}_\infty^{\mathrm{T}}(\mathbf{r}, \theta, \omega)\rangle] = \left(\frac{\omega^2}{4\pi c^2\epsilon_0}\right)^2\frac{|\alpha(\omega)|^2}{s^2}\mathrm{tr}[\mathbf{M}(\theta)\mathbf{\Phi}(\mathbf{r}_0, \omega)], \tag{12}$$

where tr denotes matrix trace. Further, the quantity $\mathbf{\Phi}(\mathbf{r}_0, \omega) = \langle \mathbf{E}^*(\mathbf{r}_0, \omega)\mathbf{E}^{\mathrm{T}}(\mathbf{r}_0, \omega)\rangle$ is the spectral SPP polarization matrix at point $\mathbf{r}_0$ which, according to Eq. (4), reads as

$$\mathbf{\Phi}(\mathbf{r}_0, \omega) = W(\omega)\mathbf{K}(\omega)e^{-2\mathbf{k}''(\omega)\cdot\mathbf{r}_0}, \tag{13}$$

with the double prime standing for the imaginary part. On combining Eqs. (12) and (13), we then get a one-to-one relationship among the SPP spectral distribution function $W(\omega)$ and the far-field spectrum $S_\infty(\mathbf{r}, \theta, \omega)$, namely,

$$W(\omega) = \left(\frac{4\pi c^2\epsilon_0}{\omega^2}\right)^2\frac{s^2}{|\alpha(\omega)|^2}\frac{e^{2\mathbf{k}''(\omega)\cdot\mathbf{r}_0}}{\mathrm{tr}[\mathbf{M}(\theta)\mathbf{K}(\omega)]}S_\infty(\mathbf{r}, \theta, \omega). \tag{14}$$

Equation (14) clearly implies that when the material parameters and the radius of the nanoscatterer are known, the spectral distribution function $W(\omega)$ and, thereby, the space–frequency and space–time coherence matrices [$\mathbf{W}(\mathbf{r}_1, \mathbf{r}_2, \omega)$ in Eq. (4) and $\mathbf{\Gamma}(\mathbf{r}_1, \mathbf{r}_2, \tau)$ in Eq. (7)], can be completely recovered from just a single spectrum measurement in the far zone. This remarkable conclusion is the main result of this Letter.

It is worthwhile to recall at this point that leakage radiation microscopy combined with Young's two-slit interferometer has earlier been employed to study SPP coherence [21,22]. These investigations, however, are restricted to a scalar treatment of the SPP field.

The spectral and temporal coherence matrices $\mathbf{W}(\mathbf{r}_1, \mathbf{r}_2, \omega)$ and $\mathbf{\Gamma}(\mathbf{r}_1, \mathbf{r}_2, \tau)$ contain all the stochastic information up to second moments of the stationary SPP field. In terms of these matrices, one may assess, for instance, the degrees of coherence in the two domains. Alternatively, one may analyze the statistical properties of light fields by employing the two-point Stokes parameters [25,26], which have specific physical interpretations similar to those of the usual (one-point) Stokes parameters and reduce to them when the two points coincide [31]. While the two-point (coherence) Stokes parameters have clear physical meanings in optical beam interferometry [32], their role in surface plasmonics is more elusive, since the SPP electric field is confined to the propagation plane [23,24]. Nevertheless, the two-point Stokes parameters associated with random SPPs are measurable and provide detailed information about the inner structure of SPP coherence, as we show below.

The four (complex-valued) two-point Stokes parameters in the space–frequency domain are introduced as [26]

$$S_n(\mathbf{r}_1, \mathbf{r}_2, \omega) = \mathrm{tr}[\mathbf{W}(\mathbf{r}_1, \mathbf{r}_2, \omega)\sigma_n], \quad n \in \{0, \ldots, 3\}, \tag{15}$$

in which σ_0 is the 2×2 identity matrix, and σ_1, σ_2, and σ_3 are the three Pauli spin matrices. The space–time domain two-point Stokes parameters could be defined analogously in terms of $\mathbf{\Gamma}(\mathbf{r}_1, \mathbf{r}_2, \tau)$ [25] or, equally, also via Eq. (7) as

$$S_n(\mathbf{r}_1, \mathbf{r}_2, \tau) = \int_0^\infty S_n(\mathbf{r}_1, \mathbf{r}_2, \omega)\mathrm{e}^{-\mathrm{i}\omega\tau}\mathrm{d}\omega, \quad n \in \{0, \ldots, 3\}. \tag{16}$$

On normalizing these parameters according to $s_n(\mathbf{r}_1, \mathbf{r}_2, \tau) = S_n(\mathbf{r}_1, \mathbf{r}_2, \tau)/[S_0(\mathbf{r}_1)S_0(\mathbf{r}_2)]^{1/2}$, where $S_0(\mathbf{r}) = S_0(\mathbf{r}, \mathbf{r}, 0)$ is the intensity at point $\mathbf{r}$, it follows that the vector-light space–time degree of coherence [33] is expressible as [32]

$$\gamma^2(\mathbf{r}_1, \mathbf{r}_2, \tau) = \frac{1}{2}\sum_{n=0}^{3} |s_n(\mathbf{r}_1, \mathbf{r}_2, \tau)|^2, \tag{17}$$

which obeys $0 \le \gamma(\mathbf{r}_1, \mathbf{r}_2, \tau) \le 1$. The degree of coherence may be similarly introduced in the space–frequency domain [32].

For the polychromatic, statistically stationary SPP fields, we find from Eqs. (4)–(6), (15), and (16) that

$$S_0(\mathbf{r}_1, \mathbf{r}_2, \tau) = \int_0^\infty W(\omega)F(\omega)\mathrm{d}\omega, \tag{18a}$$

$$S_1(\mathbf{r}_1, \mathbf{r}_2, \tau) = \int_0^\infty W(\omega)\frac{|k_z(\omega)|^2 - |k_x(\omega)|^2}{|\mathbf{k}(\omega)|^2}F(\omega)\mathrm{d}\omega, \tag{18b}$$

$$S_2(\mathbf{r}_1, \mathbf{r}_2, \tau) = \int_0^\infty W(\omega)\frac{-2[k_x^*(\omega)k_z(\omega)]'}{|\mathbf{k}(\omega)|^2}F(\omega)\mathrm{d}\omega, \tag{18c}$$

$$S_3(\mathbf{r}_1, \mathbf{r}_2, \tau) = \int_0^\infty W(\omega)\frac{2[k_x^*(\omega)k_z(\omega)]''}{|\mathbf{k}(\omega)|^2}F(\omega)\mathrm{d}\omega, \tag{18d}$$

where the prime denotes the real part, and the double prime denotes the imaginary part, as before, and the space- and time-dependent exponential function is abbreviated as

$$F(\omega) = F(\omega; \mathbf{r}_1, \mathbf{r}_2, \tau) = \mathrm{e}^{\mathrm{i}[\mathbf{k}(\omega)\cdot\mathbf{r}_2 - \mathbf{k}^*(\omega)\cdot\mathbf{r}_1 - \omega\tau]}. \tag{19}$$

Equations (18a)–(18d) show explicitly that the two-point (and one-point) Stokes parameters of stationary SPPs are determined by the spectral distribution function $W(\omega)$, which is obtained from the nanoscattered far-zone spectrum measurement.

We next examine the polychromatic SPP-field correlations in terms of the degree of coherence and the associated Stokes parameter decomposition [Eq. (17)] by two physical examples: an SPP field of broadband Gaussian (wavelength) spectrum and an SPP field composed of two mutually uncorrelated spectral components [24]. Since the SPP field decays exponentially away from the boundary, it is appropriate to consider longitudinal coherence on or very close to the interface. Therefore, in both examples, we set $z_1 = z_2 = 0$, let $x_1 = 0$ represent the SPP excitation point, denote $x_2 = x$ (see Fig. 1), and assess the equal-time ($\tau = 0$) longitudinal degree of coherence $\gamma(x)$ with regard to the normalized two-point Stokes parameters $s_n(x)$ obtained from Eqs. (18a)–(18d).

Figure 2 illustrates the structure of $\gamma(x)$ at an Ag–air interface for an SPP field with a Gaussian wavelength spectrum of the width $\Delta\lambda = 20$ nm, centered at the HeNe line $\lambda_0 = 632.8$ nm. Since the SPP propagation distance $l_{\mathrm{SPP}}(\omega) = 1/k_x''(\omega)$ at the mean wavelength is $l_{\mathrm{SPP}}(\lambda_0) = 67.7\lambda_0$, we see that the longitudinal coherence vanishes long before the wideband SPP field decays away. Figure 3, on the other hand, illustrates a situation with a persistent, long-range coherence modulation. In this figure, the decomposition of $\gamma(x)$ is shown for two independent SPP modes at Kr-laser wavelengths $\lambda_1 = 676.4$ nm and $\lambda_2 = 647.1$ nm excited on an Ag–air interface. The SPP propagation lengths are $l_{\mathrm{SPP}}(\lambda_1) = 58.0$ μm and $l_{\mathrm{SPP}}(\lambda_2) = 46.8$ μm, and we now see that, although the longitudinal coherence oscillates strongly, it survives over a range much larger than the propagation distances of the SPPs. The strong coherence modulation arises from electromagnetic similarity and is not strictly periodic due to the slightly different polarization states and decay rates of the two modes [24].

We observe from Figs. 2 and 3 that, apart from $|s_0(x)|$, which describes the sum of the x- and z-polarized field correlations between points (0,0) and $(x, 0)$, the main constituent of $\gamma(x)$ is $|s_1(x)|$, i.e., the measure of the z-polarized field correlations over the x-polarized ones and, to a lesser degree $|s_3(x)|$, which indicates an excess of correlations among the circularly polarized field components [31]. The contribution from $|s_2(x)|$, corresponding to correlations in the $\pm\pi/4$-polarized field

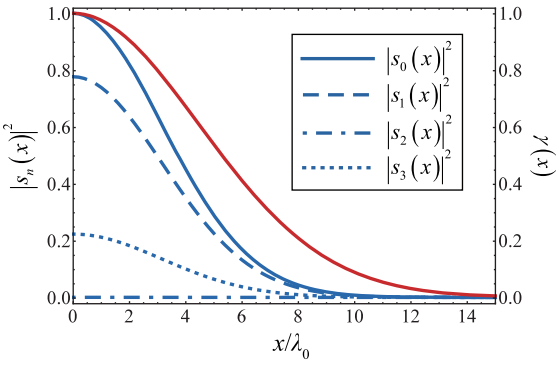

Fig. 2. Squared magnitudes of the normalized two-point Stokes parameters $s_n(x)$, with $n \in \{0, \ldots, 3\}$ (blue lines; see the inset for a legend), for a wideband Gaussian SPP field of central wavelength $\lambda_0 = 632.8$ nm and spectral width $\Delta\lambda = 20$ nm at an Ag–air interface. The solid red curve is the equal-time degree of longitudinal coherence $\gamma(x)$. The empirical data are used for the relative permittivity of Ag [34].

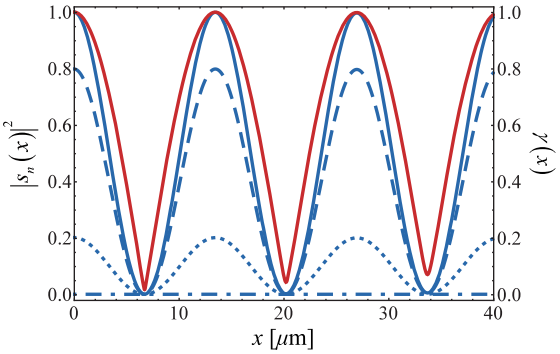

Fig. 3. Squared magnitudes of the normalized two-point Stokes parameters $s_n(x)$, with $n \in \{0, \ldots, 3\}$, as well as the equal-time degree of longitudinal coherence $\gamma(x)$, in the case of an SPP field excited by two independent Kr lasers of wavelengths $\lambda_1 = 676.4$ nm and $\lambda_2 = 647.1$ nm at an Ag–air interface. The labeling of all the curves is as in Fig. 2, and the relative permittivity of Ag is obtained from empirical data [34].

components, is seen to be negligible in both the Gaussian and the two-mode cases. These properties are a reflection of the SPP electric field being almost linearly polarized in the z direction, as is the fact that the degree of polarization is nearly unity, even for broadband SPP fields [24].

In summary, we have demonstrated theoretically that all the electromagnetic coherence properties of polychromatic, statistically stationary SPPs can be recovered from a spectrum measurement in the far zone of a dipolar nanoprobe placed in the vicinity of the metal surface in the Kretschmann setup. In analogy with related quantities for paraxial fields, we also introduced for the first time, to the best of our knowledge, the two-point Stokes parameters for such SPPs, and analyzed the intrinsic structure of the degree of coherence in the case of spectrally broadband SPPs and an SPP field consisting of two independent modes. Our simple and robust protocol for coherence measurement and assessment will be useful in applications where plasmon coherence engineering is used.

Funding. China Scholarship Council (CSC) (201606920057); Natural Sciences and Engineering Research Council of Canada (NSERC); Academy of Finland (268480).

Acknowledgment. S. Ponomarenko thanks the Joensuu University Foundation, and A. Norrman thanks the Jenny and Antti Wihuri Foundation, the Emil Aaltonen Foundation, and the Swedish Cultural Foundation in Finland for financial support.

REFERENCES

1. S. A. Maier, *Plasmonics: Fundamentals and Applications* (Springer, 2007).
2. L. Novotny and B. Hecht, *Principles of Nano-Optics*, 2nd ed. (Cambridge University, 2012).
3. A. A. Maradudin, J. R. Sambles, and W. L. Barnes, *Modern Plasmonics* (Elsevier, 2014).
4. M. Ozaki, J. I. Kato, and S. Kawata, Science **332**, 218 (2011).
5. I. Dolev, I. Epstein, and A. Arie, Phys. Rev. Lett. **109**, 203903 (2012).
6. P. Berini and I. De Leon, Nat. Photonics **6**, 16 (2012).
7. M. Kauranen and A. V. Zayats, Nat. Photonics **6**, 737 (2012).
8. A. N. Grigorenko, M. Polini, and K. S. Novoselov, Nat. Photonics **6**, 749 (2012).
9. M. S. Tame, K. R. McEnery, S. K. Özdemir, J. Lee, S. A. Maier, and M. S. Kim, Nat. Phys. **9**, 329 (2013).
10. P. Berini, Laser Photon. Rev. **8**, 197 (2014).
11. F. Che, S. A. Ponomarenko, and M. Cada, J. Opt. **18**, 125503 (2016).
12. T. W. Ebbesen, H. J. Lezec, H. F. Ghaemi, T. Thio, and P. A. Wolff, Nature **391**, 667 (1998).
13. C. H. Gan, G. Gbur, and T. D. Visser, Phys. Rev. Lett. **98**, 043908 (2007).
14. C. H. Gan, Y. Gu, T. D. Visser, and G. Gbur, Plasmonics **7**, 313 (2012).
15. S. Divitt, M. Frimmer, T. D. Visser, and L. Novotny, Opt. Lett. **41**, 3094 (2016).
16. D. Morrill, D. Li, and D. Pacifici, Nat. Photonics **10**, 681 (2016).
17. R. Carminati and J.-J. Greffet, Phys. Rev. Lett. **82**, 1660 (1999).
18. A. V. Shchegrov, K. Joulain, R. Carminati, and J.-J. Greffet, Phys. Rev. Lett. **85**, 1548 (2000).
19. T. Setälä, M. Kaivola, and A. T. Friberg, Phys. Rev. Lett. **88**, 123902 (2002).
20. L. Mandel and E. Wolf, *Optical Coherence and Quantum Optics* (Cambridge University, 1995).
21. S. Aberra Guebrou, J. Laverdant, C. Symonds, S. Vignoli, and J. Bellessa, Opt. Lett. **37**, 2139 (2012).
22. J. Laverdant, S. Aberra Guebrou, F. Bessueille, C. Symonds, and J. Bellessa, J. Opt. Soc. Am. A **31**, 1067 (2014).
23. A. Norrman, T. Setälä, and A. T. Friberg, Opt. Express **23**, 20696 (2015).
24. A. Norrman, S. A. Ponomarenko, and A. T. Friberg, Europhys. Lett. **116**, 64001 (2016).
25. J. Ellis and A. Dogariu, Opt. Lett. **29**, 536 (2004).
26. O. Korotkova and E. Wolf, Opt. Lett. **30**, 198 (2005).
27. A. Norrman, T. Setälä, and A. T. Friberg, Opt. Lett. **38**, 1119 (2013).
28. A. Norrman, T. Setälä, and A. T. Friberg, Phys. Rev. A **90**, 053849 (2014).
29. J. Tervo, T. Setälä, and A. T. Friberg, J. Opt. Soc. Am. A **21**, 2205 (2004).
30. L.-P. Leppänen, K. Saastamoinen, J. Lehtolahti, A. T. Friberg, and T. Setälä, Opt. Express **24**, 1472 (2016).
31. J. Tervo, T. Setälä, A. Roueff, P. Réfrégier, and A. T. Friberg, Opt. Lett. **34**, 3074 (2009).
32. A. T. Friberg and T. Setälä, J. Opt. Soc. Am. A **33**, 2431 (2016).
33. J. Tervo, T. Setälä, and A. T. Friberg, Opt. Express **11**, 1137 (2003).
34. E. D. Palik, ed., *Handbook of Optical Constants of Solids* (Academic, 1998).